PCCP

PAPER

View Article Online
View Journal | View Issue

Cite this: *Phys. Chem. Chem. Phys.*, 2017, **19**, 1441

Thermodynamic origins of the solvent-dependent stability of lithium polysulfides from first principles†

Tod A Pascal,*[a] Kevin H. Wujcik,[bc] Dunyang Rita Wang,[cd] Nitash P. Balsara[bce] and David Prendergast*[a]

Received 7th October 2016,
Accepted 30th November 2016

DOI: 10.1039/c6cp06889h

www.rsc.org/pccp

An understanding of the complex solution phase chemistry of dissolved lithium polysulfides is critical to approaches aimed at improving the cyclability and commercial viability of lithium sulfur batteries. Experimental measurements are frustrated by the versatile sulfur–sulfur bond, with spontaneous disproportionation and interconversion leading to unknown equilibrium distributions of polysulfides with varying lengths and charge states. Here, the solubility of isolated lithium polysulfides is calculated from first-principles molecular dynamics simulations. We explore the associated changes in the dissolution free energy, enthalpy and entropy in two regimes: liquid-phase monodentate solvation in dimethylformamide (DMF) and polymer-like chelation in bis(2-methoxyethyl) ether (diglyme). In both of these technologically relevant solvents, we show that the competition between enthalpy and entropy, related to specific interfacial atomic interactions, conspires to increase the relative stability of long chain dianionic species, which exist as Li^+–LiS_x^- contact-ion-pairs. Further, we propose a mechanism of radical polysulfide stabilization in simple solvents through the reorientation of the 1st shell solvent molecules to screen electrostatic fields emanating from the solute and explain nonmonotonicity of the dissolution entropy with polysulfide length in terms of a three-shell solvation model. Our analysis provides statistical dynamics insights into polylsulfide stability, useful to understand or predict the relevant chemical species present in the solvent at low concentrations.

Introduction

Rechargeable lithium sulfur (Li–S) batteries are based on the electrochemically reversible reaction of lithium with sulfur. They are a particularly promising technology, with a theoretical capacity of 1675 mA h g^{-1} and an energy density of 2600 W h kg^{-1},[1] both of which already satisfy the energy requirements of the 2020 US DOE goals for transportation.[2] The higher chemical potential of lithium at the anode is the thermodynamic driving force for discharge in these cells, effecting an electronic current through the external circuit and releasing lithium ions into the electrolyte. A potential difference is required to reverse the process during the charging cycle. During discharge, the electrons and lithium ions meet at the cathode and convert sulfur to lithium sulfide Li_2S:

$$16Li^+ + S_8 + 16e^- \rightarrow 8Li_2S \quad (1)$$

This overall reaction requires an octasulfur molecule, S_8 – a cyclic molecule that is the molecular constituent of rhombohedral sulfur, the thermodynamically stable allotrope of sulfur at ambient conditions – to react with sixteen lithium ions and electrons. Unfortunately, both sulfur and lithium sulfide are insulating, implying that the initiation of the discharge and charge process must be interfacially limited, potentially leading to electrically isolated material and hence a reduced capacity. Critical to the recyclability and high theoretical capacity of these cells is the conservation of electrical contact between the end-points of the cathode reaction and some conductive binder and/or the current collector. In addition, the reaction in eqn (1) proceeds in multiple steps[3] producing a distribution of lithium polysulfides,[4,5] which could be in the form of dianions (S_x^{2-}) or radical anions (S_x^-) in combination with two or one Li^+ cations, respectively. These polysulfides are soluble in typical battery electrolytes and would be expected to diffuse out of electrical contact with the cathode during cycling. This further reduces the accessible capacity and also promotes parasitic side reactions[6–8] at the anode surface

[a] *Molecular Foundry, Lawrence Berkeley National Lab, Berkeley, CA 94720, USA. E-mail: tapascal@lbl.gov, dgprendergast@lbl.gov*
[b] *Department of Chemical and Biomolecular Engineering, University of California, Berkeley, California 94720, USA*
[c] *Materials Sciences Division, Lawrence Berkeley National Laboratory, Berkeley, California 94720, USA*
[d] *Department of Materials Science and Engineering, University of California, Berkeley, California, 94720, USA*
[e] *Energy Technologies Area, Lawrence Berkeley National Laboratory, Berkeley, California 94720, USA*

† Electronic supplementary information (ESI) available: Tables S1–S5, Fig. S1–S3 and details of the 2PT method. See DOI: 10.1039/c6cp06889h

which lead to infinite charging. Unchecked, these aspects of Li–S chemistry combine to shut down the cell.

Methods of addressing polysulfide dissolution in Li–S batteries have focused on mechanical confinement strategies in graphitic materials,[1–3] and the development of electrolyte materials that block dissolution, while permitting lithium ion diffusion, through chemical functionalization.[4] Yet, the physics of polysulfide dissolution is still unknown, as is the exact chemical nature and distribution of polysulfide molecules in the bulk electrolyte. Furthermore, while the solubility of octasulfur in some common organic solvents has been measured,[5,6] the solubility of specific polysulfides is not known, in part due to an inability to isolate them. Disproportionation and interconversion reactions lead, invariably, to polysulfide mixtures with compositions presumably determined by the relative amount of lithium to sulfur and the chemical potential of the individual polysulfide molecules.

As a first step to ultimately determining the electrochemical speciation in Li–S cells, in this contribution we present the thermodynamics of 15 isolated lithium polysulfide species in the dilute limit in two common solvents, using first-principles computer simulations and free energy calculations that explicitly account for changes in the polysulfide and solvent entropy upon dissolution. We show that the intrinsic stability of dissolved polysulfides can be rationalized by consideration of the solvent structure and dynamics at equilibrium. Our investigations are centered on molecular dynamics (MD) simulations with explicit consideration of the electronic degrees of freedom of the system, calculated "on the fly" during the hamiltonian dynamics of the ionic nuclei, *i.e.*, so-called first-principles molecular dynamics (FPMD). The advantage of this approach over purely classical MD simulations, employing empirical, analytic interaction potentials, is that the system internal energy and interatomic forces are obtained from ground state electronic structure calculations. Of course this improved description of the physics incurs significant increased computational cost, which restricts the system size to the nanometer scale and the total simulation time to pico-seconds. This in turn limits the ability to calculate the Gibbs "free" energy of the system, which comprises the enthalpy (usually and somewhat trivially obtained from total energies in the FPMD simulations) and the entropy, which requires extensive sampling[7,8] – at least 2 orders of magnitude longer than practical in FPMD. Here, we overcome this limitation by approximating the total system entropy using the autocorrelation function of the atomic velocities as described in the Two-Phase Thermodynamics (2PT) method of Goddard and coworkers,[9–11] which has been shown to produce converged entropies in condensed phase systems on picosecond timescales.

Computational methods

Classical molecular dynamics simulations

Classical MD simulations were performed on each dissolved polysulfide system using the LAMMPS MD engine.[12,13] We described the DMF, diglyme and lithium polysulfide molecules using the OPLS AA/L[14,15] forcefield, which reproduces the properties of the pure systems reasonably well (Table S1, ESI†). Long-range coulombic interactions were included using the particle-particle particle-mesh Ewald method[16] (with a precision of 10^{-5} kcal mol^{-1}), while the van der Waals interactions were computed with a cubic spline (inner cutoff of 11 Å and outer cutoff of 12 Å). We used a spline to guarantee that the energies and forces go smoothly to zero at the outer cutoff, preventing any energy drift that may occur due to inconsistent forces.

The systems were then equilibrated according to our previous studies.[17–19] Briefly, after initial conjugant gradient minimization at a force tolerance of 10^{-4} kcal mol^{-1} Å^{-2}, the system was slowly heated from 0 K to 298 K with a Langevin thermostat in the constant temperature, constant volume micro-canonical (NVT) ensemble. The temperature coupling constant was 0.1 ps and the simulation timestep was 1.0 fs.

The equilibration was followed by 1ns of constant-pressure (iso-baric), constant-temperature (*NPT*) dynamics at 298 K and 1 atm. The temperature coupling constant was 0.1ps while the pressure piston constant was 2.0 ps. The equations of motion used are those of Shinoda *et al.*,[20] which combine the hydrostatic equations of Martyna *et al.*[21] with the strain energy proposed by Parrinello and Rahman.[22] The time integration schemes closely follow the time-reversible measure-preserving Verlet integrators derived by Tuckerman *et al.*[23] Production dynamics were then evolved for a further 2.5 ns in the *NPT* ensemble.

First-principles MD simulations and free energy calculations

Five uncorrelated snapshots (*i.e.*, set of atomic coordinates and velocities) of the equilibrated polysulfide system were obtained, each spaced 0.5 ns apart in the 2.5 ns production run. Each snapshot was then used as input to an FPMD simulation, performed using a modified version of the mixed Gaussian and plane wave code CP2K/Quickstep.[24,25] We employed a triple-ζ basis set with two additional sets of polarization functions (TZV2P)[26] and a 320 Ry plane-wave cutoff. The PBE functional was employed,[27] and the Brillouin zone sampled at the Γ-point only, as is customary and reasonable for the wide-band gap, disordered, condensed phase system considered here. Interactions between the valence electrons and the ionic cores are described by norm-conserving pseudopotentials.[28,29] Solutions to the Poisson equation are provided by an efficient Wavelet-based solver.[30] We overcome the poor description of the long-range dispersive forces within the PBE-GGA exchange–correlation functional by employing the DFTD3 empirical corrections of Grimme *et al.*[31] For each system, we performed at least 25 ps of constant volume constant temperature (*NVT*) dynamics, saving a snapshot of the system (atomic coordinates and velocities) at every step. The temperature of the system was kept near 300 K using a Nose–Hoover thermostat (temperature damping constant of 100 fs). In total, this represents over 3.5 ns of total simulation time and nearly 3 million computing hours. We allowed for 15 ps of equilibration and used the atomic positions and velocities from the last 10 ps of dynamics as input to an external code that performed the 2PT analysis.

Results and discussion

We focus on isolated lithium polysulfide molecules dissolved in either 16 diethylene glycol dimethyl ether (diglyme) or 27 dimethylformamide (DMF) molecules. Both of these solvents are frequently used in Li–S batteries and, as we will show below, represent two different solvation regimes: (1) liquid-like monodentate solvation by DMF, where the dissolved lithium is potentially coordinated by one carbonyl per solvent molecule, and (2) polymer-like solvation and lithium chelation in diglyme *via* its multiple ether moieties. The individual polysulfides maintained their fidelity throughout the FPMD simulations; no spontaneous disproportionation events were observed. Separately, we calculated the thermodynamic properties of the reference systems at 298 K: α-sulfur (cyclo-S_8) in its rhombohedral crystal structure; a $2 \times 2 \times 2$ supercell of the cubic lithium sulfide crystal structure; and the bulk solvents. As a figure of merit, the calculated standard molar entropy, a comprehensive measure of the dynamics and vibrational density of states, is compared to experimental measurements in Table S1 of ESI.† The thermodynamics of these homogeneous systems is as accurately reproduced in our FPMD as it is with classical forcefields parameterized to reproduce the experimental densities.

Direct validation of our computational approach is obtained by considering the solubility of S_8 in each of the two solvents. Following the lead of Truhlar and coworkers,[32] the solubility can be predicted from solvation free energies and vapor pressures: within the limits of unitary activity coefficients and solutions that obey Henry's law, the solubility of molecular S_8 is given by:

$$\frac{P_A}{\rho_0} e^{\frac{-\Delta G}{RT}} \quad (2)$$

where the sulfur vapor pressure $P_A = 0.01$ Pa,[33] ρ_0 is the pressure of an ideal gas at 1 M concentration and 298 K (*i.e.* 2.47 MPa) and ΔG is the solvation free energy (comprising enthalpic and entropic contributions, $\Delta G = \Delta H - T\Delta S$). For our purposes, dissolution free energy is the desired quantity, which is taken as the difference between the calculated absolute free energy of S_8 in the reference crystal and solution phases.

The results of our free energy calculations are given in Table 1. In DMF, we calculate a dissolution free energy $\Delta G = -34.77 \pm 1.57$ kJ mol^{-1}, which we find arises from an enthalpic cost $\Delta H = 49.21 \pm 0.99$ kJ mol^{-1}, but a significant entropic gain $T\Delta S = 83.97 \pm 8.22$ kJ mol^{-1}. The entropic gain results not only from the expected "liberation" and self-diffusion of the sulfur molecules in solution, but mostly from a disruption of the DMF liquid structure around the solute. Using eqn (2) leads to a calculated solubility of 5 mM, in excellent agreement with a recent experimental measurement of 5.9 mM[6]. Similar calculations in diglyme resulted in $\Delta G = -35.93 \pm 4.14$ kJ mol^{-1}, and a calculated solubility of 8.0 mM, again in good agreement with experimental values of 7[5], 10.2 mM[6]. As in the case of DMF, in diglyme the solubility is also driven by a significant increase in solvent entropy (the S_8 entropy increases only about as much as in DMF). As a counter example, we calculated the dissolution free energy and solubility of molecular Li_2S in each solvent. In either case, we found Li_2S to be completely insoluble, with $\Delta G = +62.21 \pm 1.23$ kJ mol^{-1} in DMF and $+45.24 \pm 3.42$ kJ mol^{-1} in diglyme. The fact that solutions of lithium polysulfides can be produced at all from solid-state reagents like S_8 and Li_2S indicates some surface chemistry on the insoluble Li_2S.

Table 1 Formation thermodynamics and solubility of S_8 in DMF and diglyme from 298 K FPMD simulations

	DMF	Diglyme
ΔG (kJ mol^{-1})	-34.77 ± 1.56	-35.93 ± 4.14
ΔH (kJ mol^{-1})	49.21 ± 0.99	166.19 ± 4.25
$T\Delta S$ (kJ mol^{-1})		
Total	83.97 ± 8.22	202.12 ± 10.14
S_8 contribution	29.27 ± 7.60	30.91 ± 4.47
Solvent contribution	54.70 ± 8.35	171.21 ± 11.67
Calc. solubility[a] (mM)	5.02 ± 0.22	8.02 ± 0.92
Expt. solubility (mM)	5.94[b]	6.98[b], 10.25[c]

[a] Using eqn (3). [b] Ref. 6. [c] Ref. 5.

Structure of lithium polysulfides in DMF

Having validated our computational approach, we turn now to the dissolution of lithium polysulfides in DMF. We find it instructive to first describe the overall equilibrium structures observed during our FPMD simulations, and then show how these structures are indicative of, and indeed result from, the underlying thermodynamics. In DMF, the equilibrium structures fall into two general families: long-chain polysulfides Li_xS_y [$5 \leq y \leq 8$] and short-chain polysulfides [$y = 2, 3$]. Fig. 1 provides representative snapshots from each family, while Fig. S1 of ESI† presents the full list. We note that these structures differ significantly from those optimized structures generated from isolated clusters without specific solvent interactions and excluding finite-temperature effects. Under those unrealistic conditions, lithium polysulfides generally form approximately linear Li–S_x–Li chains, so as to minimize Li^+–Li^+ electrostatic repulsion.[34] In explicit solvent, there are specific interactions between the solvent's electronegative coordinating groups (carbonyl oxygens in the case of DMF) which compete with the sulfur molecules for the lithium ions. These effects are not captured in the gas phase nor even in implicit solvent models.

As a generalized metric to describe the lithium polysulfide equilibrium structure in solution, we performed structural analysis, by means of pair distribution functions. This revealed that for the short-chain polysulfide dianions, each lithium atom is coordinated in a quasi-tetrahedral arrangement by two sulfur and two solvent oxygen atoms (Fig. 1c, Fig. S2 and Table S2, ESI†). The partial atomic charge on the terminal sulfur atoms[35] ranges from $-1e^-$ (S_2^{2-}) to $-0.735e^-$ (S_3^{2-}), lending these sites competitive electrostatic interactions with the lithium ion with respect to the DMF carbonyl oxygen. Therefore, the most electrostatically favored configuration is one that maximizes the sulfur–lithium electrostatic interactions, while at the same time minimizing lithium–lithium repulsion.

For the longer-chain polysulfide dianions, the equilibrium structures diverge from a tetrahedral lithium coordination. We note that, schematically, polysulfide dianions are described as

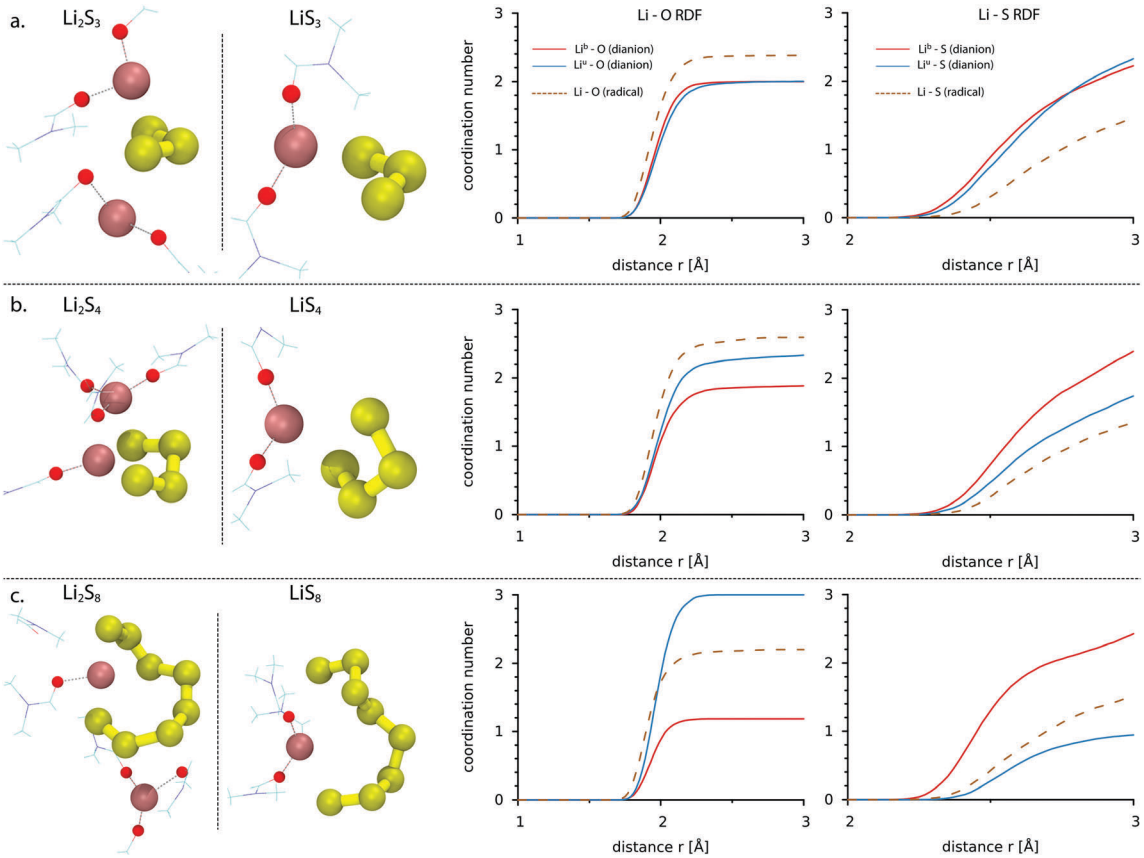

Fig. 1 (a) From left to right: representative equilibrium snapshots of Li_2S_x and LiS_x in DMF, Li–O and Li–S radial distribution functions (RDFs). In the snapshots, the lithium ions (pink), sulfur (yellow) and coordinating oxygen (red) atoms are emphasized. In the RDFs for the dianions, we separately consider the "unbound" (Li^u) and "bound" (Li^b) lithium ions. (b) Snapshots and RDFs for Li_xS_4 (c) snapshots and RDFs for Li_xS_8.

having neutral internal atoms and termini each with a charge of $-1e^-$. However as we have shown previously, the two electrons defining the charge of the dianion are delocalized over every sulfur atom, albeit with maxima at the termini, and, with increasing chain length and delocalization, the local electronic charge on each sulfur atom decreases.[35] Therefore, the long-chained polysulfides exhibit reduced Li–S binding (increased lithium ion mobility) and reduced overall electrostatic repulsion between negatively charged sulfur atoms in the polysulfide and similarly charged oxygen atoms in the solvent molecules. The net result of these competing effects is an equilibrium structure with two distinct lithium cations: a "bound" lithium ion, tightly coordinated by the sulfur molecule (coordination numbers of 3 and 1 for S and O, respectively – Table S3, ESI†), and an "unbound" lithium ion, predominantly coordinated by the solvent (coordination numbers of 1 and 3 with S and O, respectively). Thus, long-chain polysulfide dianions more closely resemble contact ion pairs, with Li^+–$Li_2S_x^-$ species. The Li ion coordination of Li_2S_4 lies intermediate between the short- and long-chain polysulfide limits. We note that the differing solvation environments around each type of lithium ion provides an alternative explanation of recent NMR observations.[36,37]

Compared to the dianions, the solvation structure of the radical anions (LiS_x) in DMF is relatively invariant with chain length. Here, the absence of a second lithium ion and the reduced sulfur partial atomic charge leads to structures with the lithium ion equally coordinated by the sulfur molecule and the DMF oxygen atoms. Thus, much like the short-chain dianions, the solution structure of the radicals is that of electrostatically neutral complexes. These differences in the equilibrium solvation structure gives rise to marked differences in thermodynamic stability, which we address presently.

In each case, on the time scale of our FPMD trajectories, we do not observe significant exchange within the solute internal structure (bound *vs.* unbound lithium, for example, maintain their coordinations). This lends itself to the concept of "solvates" within lithium polysulfide solutions, which effectively freeze in particular long-lived coordinations, with significant consequences for the entropic contributions to the dissolution free energy, as we shall see below.

Thermodynamics of lithium polysulfides in DMF

When considering the energies of dissolved lithium polysulfides in bulk solvent (in the dilute limit), one should consider dissolution of the reagents with necessary reactions. Equivalently, from a thermodynamic standpoint, and for computational convenience, we consider two separate processes: (1) the solid-phase formation energy of each solid polysulfide from the reference solids; and (2)

the energy to dissolve this solid polysulfide in the bulk solvent. Both of these processes can be combined to give a "dissolution and reaction" energy according to master equations for the dianions:

$$\mathrm{Li_2S^{(s)}} + \frac{(x-1)}{8}\mathrm{S_8^{(s)}} + \mathrm{solvent}^{(l)} \rightarrow \mathrm{Li_2S_x^{(solv)}} \qquad (3)$$

and for the radicals:

$$\mathrm{Li_2S^{(s)}} + \frac{(2x-1)}{8}\mathrm{S_8^{(s)}} + 2 \times \mathrm{solvent}^{(l)} \rightarrow 2\mathrm{LiS_x^{(solv)}} \qquad (4)$$

The thermodynamics of each species (in its stated phase) in eqn (3) and (4) above can be obtained independently, greatly simplifying our calculations.

Consider first the thermodynamics of forming and dissolving the polysulfide dianions in DMF. As shown in Fig. 2 and Table S4 (ESI†), the dissolution free energy (and thus solubility) of the dianions increases with increasing chain length. Indeed, Li_2S_2 has a positive dissolution free energy (*i.e.*, would be insoluble according to eqn (2)), while Li_2S_6–Li_2S_8 have dissolution free energies ~ -50 kJ mol^{-1} molecule^{-1}, which would correspond to 1.5–3 M solubility if eqn (2) is applied directly. The enthalpy of polysulfide dissolution is always favorable, a natural consequence of the attractive electrostatic interactions of the charged sulfur molecules and lithium ions with the polar solvent. Less expected are the changes in the entropy of dissolution, which are positive for the shorter-chain dianions but progressively more negative with increasing chain length.

The peculiar entropy of polysulfide dianion dissolution in DMF results from underlying changes in the solvent dynamics. To quantify this effect, we calculated the distribution of molecular entropies of each DMF molecule (Fig. 3a), according to their distance from the lithium polysulfide. We found that DMF molecules in the first solvation shell (*i.e.*, molecules within 2.5 Å of the sulfur molecule or lithium ions) had increased entropy (by $\sim$10 J mol^{-1} K^{-1} or $\sim$5%) with respect to the bulk solvent (Fig. 3b), due primarily to enhanced librations from coupling to the mobile lithium ions. This is exemplified in Fig. S3 (ESI†) as enhancement in the density of states function between 230–500 cm^{-1}, corresponding to motions in the lithium ions at similar frequencies. By contrast, molecules in the second solvation shell had lower entropy than the bulk ($\sim$3%).

We thus propose a three-shell model of lithium polysulfide solvation in liquid-like, monodentate solvents. For short-chain polysulfides, a larger number of DMF molecules lie in the first solvation shell than in the second shell, leading to an increase in total entropy of the system. The number of less entropically stable second shell molecules increases faster than the more entropically stable first shell molecules with increasing polysulfide length (size) however. Therefore, in the longer-chain polysulfides, the overall dissolution entropy is negative. A similar, but opposite, entropy model has been proposed for a DNA triplex[38] in salt water.

The dissolution free energy of the dianions can be contrasted with that of the radicals. Generally, we find that the solvated radicals are less stable than the dianions, with solubilities in the mM range. Additionally, the radical dissolution free energies are not a linear function of polysulfide chain length. Analysis of the two energy terms revealed that, apart from LiS_2 which is insoluble, the dissolution enthalpy is less negative than for the dianions (there are fewer possible Li^+–DMF interactions) and is relatively constant with radical chain length. Additionally, the dissolution entropy losses in the radical anions are larger than in the corresponding dianion. Here, in contrast to the dianions again, the entropy of the first solvation shell DMF molecules is lower than the bulk (Fig. 3c and d), the result of a change in solvent dynamics where the first-shell DMF molecules preferentially reorient to screen the more uniform electrostatic environment presented by the rigid LiS_x motif. The net effect is a predicted radical stability of $S_3^- > S_4^- > S_6^- > S_8^- > S_5^- > S_7^- \gg S_2^-$. Note that the relative stability of the S_3^- radical in DMF is due to it having the best compromise between favorable relative enthalpy and low entropy loss. Spectroscopic and paramagnetic measurements[39–42] have long detected the presence of

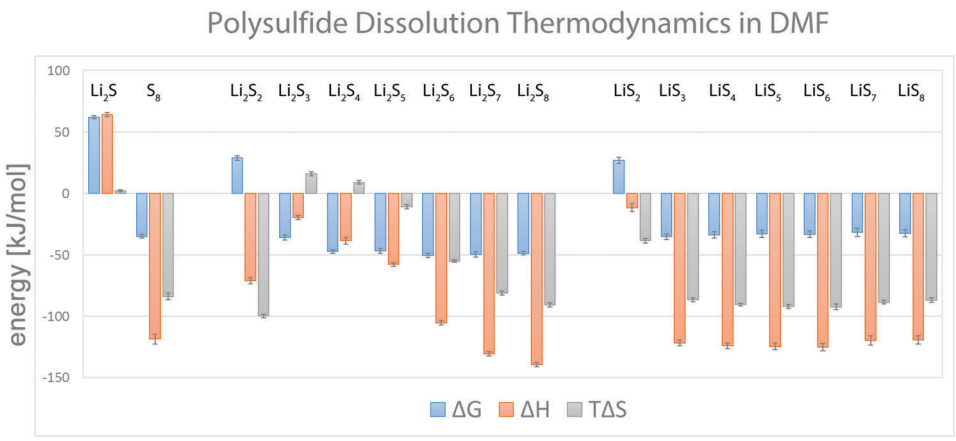

Fig. 2 Thermodynamics of dissolution of various lithium polysulfides in DMF. The relative Gibbs free energy (ΔG - blue), enthalpy (ΔH - orange) and total entropy ($T\Delta S$ - grey) are obtained according to eqn (3) and (4). The free energy of dissolution of the crystalline solid starting materials (Li_2S and S_8) are provided for reference.

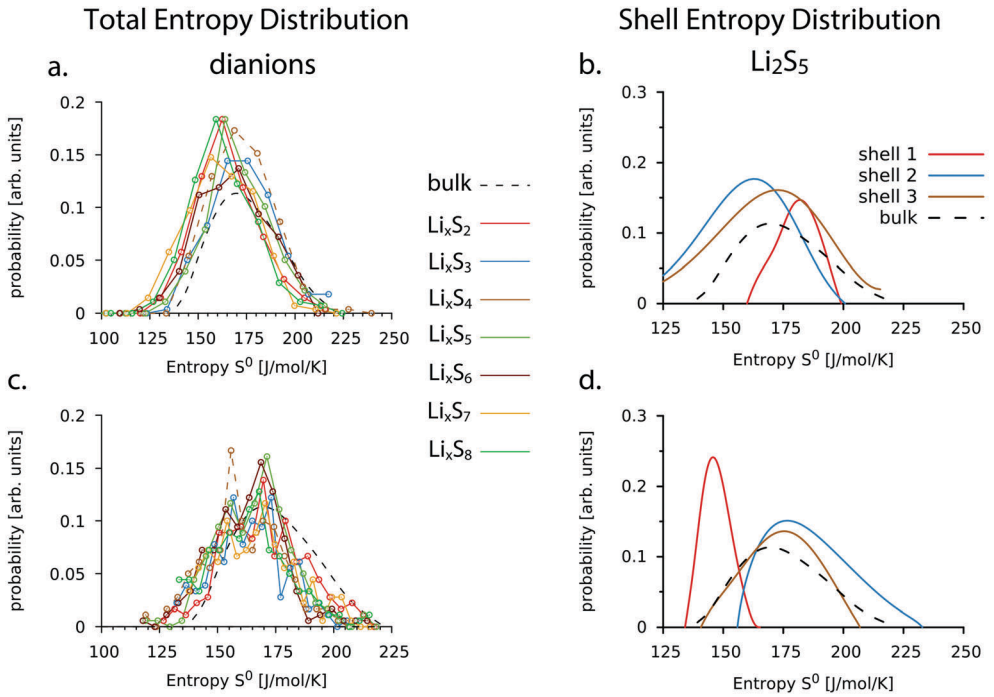

Fig. 3 Distribution of DMF entropies in dissolved polysulfides (a) distribution of entropy of DMF solvent molecules in lithium dianion polysulfide solutions (x = 2). The entropy distribution of the bulk solvent (dashed black line) is referenced. (b) Distribution of DMF entropy as a function of distance from the Li atoms (shells) for Li_2S_5 (c) distribution of entropy of DMF molecules in lithium radical solutions (x = 1). (d) DMF shell entropy distribution for LiS_5.

radical anions in DMF. However, to date, there has not been any definitive proof or explanation of S_3^- being the dominant radical species.

Comparison of lithium polysulfide structure in digylme and DMF

Diglyme molecules, being a practical model of polymer-like solvation in longer chain polyethers, are larger and less polar, leading to a more viscous solvent that DMF. The lithium ions interact primarily with the ether oxygens on diglyme, resulting in a fairly rigid solvate (*i.e.* the polysulfide and its associated, chelating diglyme molecules Fig. 4a). In contrast to DMF, in diglyme both short- and long-chain polysulfide dianions exhibit ratios of lithium–oxygen to lithium–sulfur coordination numbers of approximately 2 : 2 and 3 : 1 for the bound and unbound lithium ions, respectively (Table S3, ESI†). The solvate size varies, depending on whether the unbound lithium ions are chelated by three oxygen atoms on the same (more common in longer chain polysulfides) or on separate diglyme molecules. In the case of the polysulfide radical, the overall equilibrium structure is less varied with chain length and is more polar than in DMF. The solvate comprises a rigid solution structure with a tightly chelated lithium ion and a 3 : 1 ratio for Li–O : Li–S coordination.

Thermodynamics of lithium polysulfides in diglyme *vs.* DMF

Fig. 4b shows the dissolution energies of the various lithium polysulfides in diglyme. While the dissolution free energy and solubility of neutral S_8 in diglyme is similar to DMF, the polysulfides are all significantly less soluble in diglyme (Table S5, ESI†) than in DMF. For example, the calculated formation free energy of the most soluble polysulfides in diglyme, Li_2S_7 and Li_2S_8, are $\sim$15 kJ mol^{-1} less than in DMF. This is the case even though the dissolution enthalpy in diglyme is more favorable than DMF – a result of the increased number of lithium–oxygen interactions ($\sim$5 in diglyme *vs.* $\sim$4 in DMF) (Table S3, ESI†). On the other hand, the losses in the dissolution entropy are far more pronounced in diglyme, owing to the rigid solvate structures with highly chelated lithium ions which greatly restricts the mobility of the associated solvent molecules and the solvate self-diffusion. The entropic losses in the radicals are even larger than in the dianions, due to the more rigid and polar solvate structure noted above, resulting in a net unfavorable free energy of dissolution.

The radical polysulfides are predicted to be relatively unstable in diglyme at room temperature, consistent with experimental spectroscopic studies.[43–47] We note, however, that our calculations do not preclude the existence of radical polysulfide anions in diglyme solutions, but rather predicts a low probability of finding isolated radicals. A chemical mixture of polysulfides in diglyme that result from a specific initial condition (either lithium or sulfur rich starting materials) could in fact contain radicals if their population prevents the formation of even more insoluble species in solution (*e.g.* Li_2S_2 or Li_2S). The ultimate usefulness of the dissolution free energy presented in this work is in determining (subject to mass and charge balance constraints) the equilibrium distribution of polysulfides that would minimize the overall free energy.

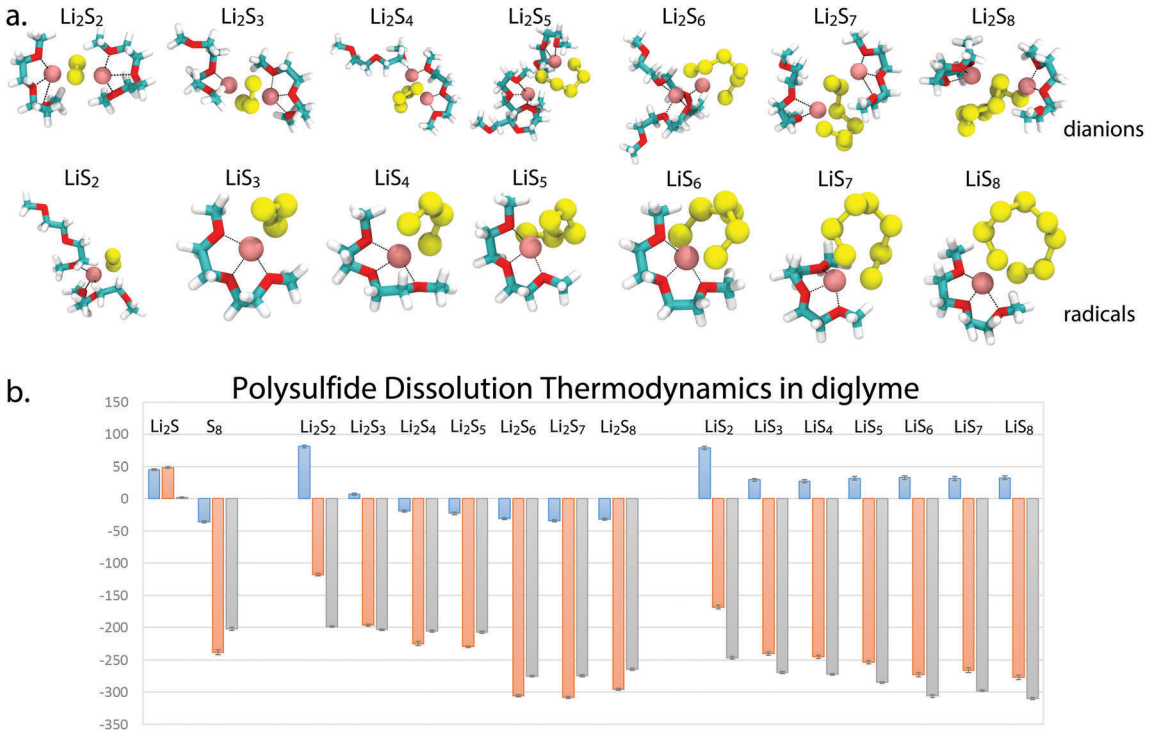

Fig. 4 (a) Representative equilibrium configurations of Li_xS_y polysulfide dianions (x = 2, top row) and radicals (x = 1, bottom row) in diglyme from 298 K FPMD simulations. (b) Formation free energy (blue), total entropy (gray) and enthalpy (orange) of lithium polysulfides dissolved in diglyme (as in Fig. 2).

Conclusions

We have shown that careful examination of the solvation dynamics at the solute–solvent interface can deepen our understanding of the relative system free energy. In this study, we utilized the 2PT approach, based solely on the auto-correlation function of the atomic velocities, to feasibly calculate converged first-principles entropies on pico-second timescales. Our results show a significant loss of entropy (and associated free-energy destabilization) associated with polysulfide dissolution, which compensates for increased lithium-solvent electrostatic interactions. These entropic losses greatly reduce the stability of dissolved lithium polysulfides, particularly that of the radical species in polymer based solvents such as diglyme. This suggests polyether solvents as good candidate components in future electrolytes aimed at reducing polysulfide dissolution through the formation of quasi-rigid solvates. Our future studies will focus on predicting lithium polysulfide speciation in solution, and determining the mechanism for disproportionation and interconversion.

Acknowledgements

This work was supported by the Assistant Secretary for Energy Efficiency and Renewable Energy, Office of Vehicle Technologies of the U.S. Department of Energy under Contract DE-AC02-05CH11231 under the Batteries for Advanced Transportation Technologies. This work was performed as a user project at the Molecular Foundry, Lawrence Berkeley National Laboratory supported by the Office of Science, Office of Basic Energy Sciences, of the U.S. Department of Energy under the same contract. Computer simulations used resources of the National Energy Research Scientific Computing Center, which is supported by the Office of Science of the U.S. Department of Energy, also under the same contract.

References

1 X. Ji, K. T. Lee and L. F. Nazar, *Nat. Mater.*, 2009, **8**, 500–506.
2 X. Liang, C. Hart, Q. Pang, A. Garsuch, T. Weiss and L. F. Nazar, *Nat. Commun.*, 2015, **6**, 5682.
3 Z. W. Seh, W. Li, J. J. Cha, G. Zheng, Y. Yang, M. T. McDowell, P.-C. Hsu and Y. Cui, *Nat. Commun.*, 2013, **4**, 1331.
4 I. Villaluenga, K. H. Wujcik, W. Tong, D. Devaux, D. H. Wong, J. M. DeSimone and N. P. Balsara, *Proc. Natl. Acad. Sci. U. S. A.*, 2016, **113**, 52–57.
5 S. F. Sciamanna and S. Lynn, *Ind. Eng. Chem. Res.*, 1988, **27**, 492–499.
6 D. Zheng, X. Zhang, C. Li, M. E. McKinnon, R. G. Sadok, D. Qu, X. Yu, H.-S. Lee, X.-Q. Yang and D. Qu, *J. Electrochem. Soc.*, 2015, **162**, A203–A206.
7 G. M. Torrie and J. P. Valleau, *J. Comput. Phys.*, 1977, **23**, 187–199.
8 X. Kong and C. L. Brooks Iii, *J. Chem. Phys.*, 1996, **105**, 2414–2423.
9 T. A. Pascal, S. T. Lin and W. A. Goddard, *Phys. Chem. Chem. Phys.*, 2011, **13**, 169–181.

10 S.-T. Lin, P. K. Maiti and W. A. Goddard, *J. Phys. Chem. B*, 2010, **114**, 8191–8198.
11 S. T. Lin, M. Blanco and W. A. Goddard, *J. Chem. Phys.*, 2003, **119**, 11792–11805.
12 S. J. Plimpton, R. Pollock and M. Stevens, Particle-Mesh Ewald and rRESPA for Parallel Molecular Dynamics Simulations, in *Proc of the Eighth SIAM Conference on Parallel Processing for Scientific Computing*, Minneapolis, MN, 1997.
13 S. Plimpton, *J. Comput. Phys.*, 1995, **117**, 1–19.
14 W. L. Jorgensen and J. Tiradorives, *J. Am. Chem. Soc.*, 1988, **110**, 1657–1666.
15 G. A. Kaminski, R. A. Friesner, J. Tirado-Rives and W. L. Jorgensen, *J. Phys. Chem. B*, 2001, **105**, 6474–6487.
16 R. W. Hockney and J. W. Eastwood, *Computer Simulation Using Particles*, Taylor & Francis, New York, 1989.
17 K. P. Maiti, T. A. Pascal, N. Vaidehi and W. A. Goddard, *J. Nanosci. Nanotechnol.*, 2007, **7**, 1712–1720.
18 P. K. Maiti, T. A. Pascal, N. Vaidehi, J. Heo and W. A. Goddard, *Biophys. J.*, 2006, **90**, 1463–1479.
19 P. K. Maiti, T. A. Pascal, N. Vaidehi and W. A. Goddard, *Nucleic Acids Res.*, 2004, **32**, 6047–6056.
20 W. Shinoda, M. Shiga and M. Mikami, *Phys. Rev. B: Condens. Matter Mater. Phys.*, 2004, **69**, 134103.
21 G. J. Martyna, D. J. Tobias and M. L. Klein, *J. Chem. Phys.*, 1994, **101**, 4177–4189.
22 M. Parrinello and A. Rahman, *J. Appl. Phys.*, 1981, **52**, 7182–7190.
23 M. E. Tuckerman, J. Alejandre, R. Lopez-Rendon, A. L. Jochim and G. J. Martyna, *J. Phys. A: Math. Gen.*, 2006, **39**, 5629–5651.
24 G. Lippert, J. Hutter and M. Parrinello, *Mol. Phys.*, 1997, **92**, 477–487.
25 J. VandeVondele, M. Krack, F. Mohamed, M. Parrinello, T. Chassaing and J. Hutter, *Comput. Phys. Commun.*, 2005, **167**, 103–128.
26 J. VandeVondele and J. Hutter, *J. Chem. Phys.*, 2007, **127**, 114105.
27 J. P. Perdew, K. Burke and M. Ernzerhof, *Phys. Rev. Lett.*, 1996, **77**, 3865–3868.
28 M. Krack, *Theor. Chem. Acc.*, 2005, **114**, 145–152.
29 S. Goedecker, M. Teter and J. Hutter, *Phys. Rev. B: Condens. Matter Mater. Phys.*, 1996, **54**, 1703–1710.
30 L. Genovese, T. Deutsch and S. Goedecker, *J. Chem. Phys.*, 2007, **127**, 054704.
31 S. Grimme, J. Antony, S. Ehrlich and H. Krieg, *J. Chem. Phys.*, 2010, **132**, 154104.
32 J. D. Thompson, C. J. Cramer and D. G. Truhlar, *J. Chem. Phys.*, 2003, **119**, 1661–1670.
33 R. Hultgren, P. D. Desai, D. T. Hawkins, M. Gleiser and K. K. Kelley, *Selected values of the thermodynamic properties of the elements*, DTIC Document, 1973.
34 M. Vijayakumar, N. Govind, E. Walter, S. D. Burton, A. Shukla, A. Devaraj, J. Xiao, J. Liu, C. Wang, A. Karim and S. Thevuthasan, *Phys. Chem. Chem. Phys.*, 2014, **16**, 10923–10932.
35 T. A. Pascal, K. H. Wujcik, J. Velasco-Velez, C. Wu, A. A. Teran, M. Kapilashrami, J. Cabana, J. Guo, M. Salmeron, N. Balsara and D. Prendergast, *J. Phys. Chem. Lett.*, 2014, **5**, 1547–1551.
36 C. Barchasz, F. Molton, C. Duboc, J.-C. Leprêtre, S. Patoux and F. Alloin, *Anal. Chem.*, 2012, **84**, 3973–3980.
37 M. Cuisinier, P.-E. Cabelguen, S. Evers, G. He, M. Kolbeck, A. Garsuch, T. Bolin, M. Balasubramanian and L. F. Nazar, *J. Phys. Chem. Lett.*, 2013, **4**, 3227–3232.
38 T. A. Pascal, W. A. Goddard, P. K. Maiti and N. Vaidehi, *J. Phys. Chem. B*, 2012, **116**, 12159–12167.
39 F. Gaillard and E. Levillain, *J. Electroanal. Chem.*, 1995, **398**, 77–87.
40 D.-H. Han, B.-S. Kim, S.-J. Choi, Y. Jung, J. Kwak and S.-M. Park, *J. Electrochem. Soc.*, 2004, **151**, E283–E290.
41 R. D. Rauh, F. S. Shuker, J. M. Marston and S. B. Brummer, *J. Inorg. Nucl. Chem.*, 1977, **39**, 1761–1766.
42 Q. Wang, J. Zheng, E. Walter, H. Pan, D. Lv, P. Zuo, H. Chen, Z. D. Deng, B. Y. Liaw, X. Yu, X. Yang, J.-G. Zhang, J. Liu and J. Xiao, *J. Electrochem. Soc.*, 2015, **162**, A474–A478.
43 S.-I. Tobishima, H. Yamamoto and M. Matsuda, *Electrochim. Acta*, 1997, **42**, 1019–1029.
44 J. M. Durand, J. OlivierFourcade, J. C. Jumas, M. Womes, C. M. Teodorescu, A. Elafif, J. M. Esteva and R. C. Karnatak, *J. Phys. B: At., Mol. Opt. Phys.*, 1996, **29**, 5773–5784.
45 V. L. Tauson, J. Goettlicher, A. N. Sapozhnikov, S. Mangold and E. E. Lustenberg, *Eur. J. Mineral.*, 2012, **24**, 133–152.
46 S. Tarling, P. Barnes and J. Klinowski, *Acta Crystallogr., Sect. B: Struct. Sci.*, 1988, **44**, 128–135.
47 M. Cuisinier, C. Hart, M. Balasubramanian, A. Garsuch and L. F. Nazar, *Adv. Energy Mater.*, 2015, **5**, 1401801.

